

# The Planck Low Frequency Instrument

N. Mandolesi<sup>1</sup>, M. Bersanelli<sup>2</sup>, C. Burigana<sup>1</sup> & F. Villa<sup>1</sup>  
On behalf of LFI Consortium

<sup>1</sup>*Istituto TeSRE, CNR, Bologna, Italy;* <sup>2</sup>*IFC, CNR, Milano, Italy.*

ABSTRACT – The Low Frequency Instrument (LFI) of the “Planck Surveyor” ESA mission will perform high-resolution imaging of the Cosmic Microwave Background anisotropies at four frequencies in the 30–100 GHz range. We review the LFI main scientific objectives, the current status of the instrument design and the on-going effort to develop software simulations of the LFI observations. In particular we discuss the design status of the PLANCK telescope, which is critical for reaching adequate effective angular resolution.

KEYWORDS: Cosmic Microwave Background – Space Missions – Telescopes.

## 1. INTRODUCTION

The Planck LFI represents the third generation of mm-wave instruments designed for space observations of CMB anisotropies, following the COBE Differential Microwave Radiometer (DMR) and the Microwave Anisotropy Probe (MAP). The DMR, launched in 1989, detected structure in the CMB angular distribution at angular scales  $> 7$  deg. The LFI will produce images of the sky at four frequencies between 30 and 100 GHz, with an unprecedented combination of sky coverage, calibration accuracy, freedom from systematic errors, stability and sensitivity (including polarized components). The LFI will produce full sky maps at 30, 44, 70 and 100 GHz, with angular resolution of  $33'$ ,  $23'$ ,  $14'$  and  $10'$ , respectively, and with an average sensitivity per resolution element  $\Delta T/T \simeq a \text{ few} \times 10^{-6}$ . These unprecedented angular resolution and sensitivity will uncover the wealth of cosmological information encoded in the anisotropy pattern at degree and sub-degree angular scales.

In the LFI frequency range the contaminating effect of the galactic emission, dominating the astrophysical foreground noise on scale  $\geq 30'$ , is minimum at around 60 GHz; while the confusion noise due to extragalactic sources, dominating on smaller angular scales, is minimum in the range 100–200 GHz, where it is primarily due to radio sources (De Zotti & Toffolatti 1998). The 70 and 100 GHz channels are therefore optimal to get the cleanest possible view of primordial CMB fluctuations, over the full range of angular scales. In both channels the astrophysical foreground noise is expected to be well below the cosmological signal for all observed angular scales. At 100 GHz then the LFI will accurately measure the power spectrum of CMB anisotropies up to multipoles  $\ell \sim 1300$  with an accuracy of the order of, or better, than 1%. Little cosmological information is left at angular scales smaller than 10 arcminutes, if standard inflationary models hold; in fact anisotropies at such scales are quasi-exponentially erased by photon diffusion.

The LFI measurements will determine of the primary cosmological parameters (Hubble constant, deceleration parameter, curvature of space, baryon density, dark matter densities including neutrinos, amplitude and spectral index of the primordial scalar density perturbations, and the gravity wave content of the Universe) to an accuracy of a few percent (see, e.g., Bond et al. 1997). The LFI data can test models for the origin of primordial perturbations, i.e. whether they are due to topological defects or to quantum fluctuations, and constrain the global properties of the Universe (topology, rotation, shear, etc.) and the theories of particle physics at energies  $\simeq 10^{16}$  GeV. Polarization measurements, which will be possible with an accuracy of a few  $\mu\text{K}$  towards the ecliptic caps, will independently confirm these findings and help in breaking degeneracy in the determination of cosmological parameters (Zaldarriaga et al. 1997). Also, constraints on (or possible detections of) deviations of the CMB spectrum from a planckian shape can be accurately studied by Planck, by analyzing the dipole signature, so providing interesting information on cosmological and astrophysical processes at high redshifts (Danese & De Zotti 1981, Burigana et al. 1998b).

The LFI will also detect the Sunyaev-Zeldovich effect (Sunyaev & Zeldovich 1970) towards a few hundred of clusters of galaxies, allowing an independent determination of the Hubble constant (Cavaliere et al. 1979; Myers et al. 1997) and providing information on the intercluster medium complementary to those from X-rays (Rephaeli 1995). The LFI four-frequency all-sky surveys will also be unique in providing complete samples comprising from several hundred to a few thousands extragalactic sources, selected in an essentially unexplored frequency range, like familiar “flat-spectrum” radiosources, sources with strongly inverted spectra and possible new classes of sources (Toffolatti et al. 1998, De Zotti & Toffolatti 1998).

Moreover, the LFI maps will provide a rich database for studies of Galactic evolution, the interstellar medium, and discrete Galactic sources, including supernova remnants, Sagittarius A, and sources self-absorbed up to high frequencies such as some symbiotic stars and planetary nebulae.

The combination of data from its two instruments, LFI and HFI (High Frequency Instrument, see Puget et al. 1998), give to the Planck Surveyor the imaging power, the redundancy and the control of systematic effects and foreground emissions needed to achieve the extraordinarily exciting scientific goals of this mission in a broad spectral range, from 30 to 857 GHz. This, in turn, is crucial for improving the accuracy in the determination of the cosmological parameters. LFI and HFI will deal primarily with different astrophysical processes, radio and dust emission, respectively, both coexisting in real astrophysical sources. The LFI data are crucial to separate the cosmic signal from the contaminating effect of extragalactic radio sources which dominate the foreground fluctuations on small angular scales in the cosmologically cleanest frequency range, at least up to 200 GHz. On the other hand, the HFI maps will be useful to subtract the Galactic dust emission which is important on intermediate to large angular scales down to 100 GHz. Also, the full set of Planck data will be essential to address a number of important astrophysical problems such as to elucidate physical and evolutionary connections between nuclear

activity (responsible for the radio emission) and processes governing the abundance and the properties of the interstellar material (responsible for the sub-mm dust emission).

## 2. PROGRAMMATICS

Planck was formerly called COBRAS/SAMBA (Bersanelli et al. 1996), a combination of the two CMB proposals “COBRAS” and “SAMBA” submitted to ESA in 1993 in response to the call for mission ideas for the Medium-Size M3 mission, expected to be launched in 2003. After the Assessment Study and Phase A Study, COBRAS/SAMBA was selected and approved in late 1996, it was renamed in honor of Max Planck and the launch was then planned for 2004. The ESA Announcement Opportunity (AO) for the instruments for the FIRST/Planck Programme was issued in 1997 announcing a launch in 2006. Budgetary pressures within ESA’s scientific programme have forced a reconsideration of the original implementation plan for Planck. Between 1997 and 1998 several studies were carried out to determine how Planck will be implemented. After we replied to the AO the launch date was shifted to 2007. The preferred option at the present time is to launch Planck together with the FIRST mission; in this solution (known as the “Carrier” configuration because of the launch arrangement) both Planck and FIRST will be placed in separate orbits around the second Lagrangian point of the Earth-Sun System. The LFI data will be transmitted to the LFI Data Processing Center (see Pasian & Gispert 1998 for a detailed description).

## 3. INSTRUMENT DESCRIPTION

A schematic overview of the LFI front-end unit is shown in Figure 1. The front-end unit is located at the focus of the Planck off-axis telescope in a circular configuration around the High Frequency Instrument. The front-end unit is the heart of the instrument, and includes 28 modules, each containing one feed horn, one orthomode transducer (OMT), two hybrid couplers, two phase switches, and four cryogenic amplifiers.

The radiation focused by the telescope is coupled to the radiometers by conical, corrugated feedhorns (Bersanelli et al. 1998, Villa et al. 1997,1998a). The radiation patterns of the horns must be highly symmetric, with low sidelobes and a beam width that matches the telescope edge taper requirement ( $< -30$  dB at 22deg). In addition, the electromagnetic field inside the horn must propagate with low attenuation and low return loss. The OMTs separate the orthogonal polarizations with minimal losses and cross-talk. The return loss ( $< -25$  dB) and the insertion loss ( $< 0.1$  to  $0.3$  dB depending on frequency) must be met over the whole 20% bandwidth.

Each OMT is coupled to an integrated front-end module containing the hybrid couplers (two for each module) and the amplifier chains including phase switches and output hybrids. The front-end modules are mounted on the 20 K plate. Each

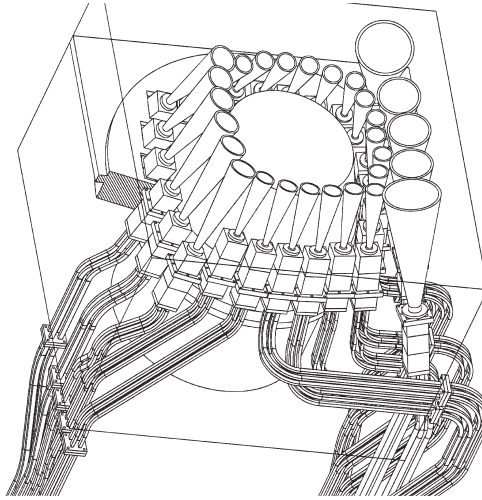


FIGURE 1. Schematic of LFI front-end unit in the asymmetric configuration.

hybrid has two inputs, one of which sees the sky through one of the OMT arms and the feed horn, the other of which looks at the 4K reference load through a small horn fabricated into the hybrid block. Four amplifiers are contained in each amplifier block, with multiple inputs and outputs on a single flange to minimize size. The hybrid coupler combines the signals from the sky and cold load with a fixed phase offset of either  $90^\circ$  or  $180^\circ$  between them. More details on the LFI receiver concept and potential systematics are given by Bersanelli & Mandolesi (1998).

The LFI Front End Unit is cooled to 20 K by a hydrogen sorption cooler (Wade & Levy 1997). In addition to meeting temperature and capacity requirements, the sorption cooler has major advantages for Planck: it is highly efficient; there are no cold moving parts, no vibration, and very low EMI; and integration with the instruments and spacecraft is simple, since the only part of the cooler in the focal assembly is a J-T valve and associated tubing while the compressor and control electronics are located remotely on the spacecraft. The sorption cooler also provides 18 K precooling to the HFI helium J-T cooler. The Planck thermal design allows efficient radiative cooling of the payload and an optimized design of the combined LFI and HFI front-end assemblies in the focal plane.

Following amplification, the signals are passed through a cryogenic, low-power phase switch, which adds  $90^\circ$  or  $180^\circ$  of phase lag to the signals thus selecting the input source as either the sky or the reference load at the radiometer output at a rate of about 1 kHz. The phase lagged pair of signals is then passed into a second hybrid coupler, separating the signals. The inclusion of the phase switches and second hybrids in the front-end blocks eliminates the need for phase matching of the long transmission paths to the back-end, greatly simplifying integration and testing.

Each cryogenic front-end module is connected with the room temperature section with four waveguides or cables, grouped together. This results in a total of 20

coax cables and 92 waveguide sections running between the front-end unit and the back-end unit. The transmission lines are further grouped into four bundles and configured to allow the required flexibility and clearance for integration of HFI in the central portion of the assembly.

Each back-end module comprises two parallel chains of amplification, filtering, detection, and integration. The detected signals are amplified and a low-pass filter or integrator reduces the variance of the random signal, providing in each channel a DC output voltage related to the average value. Post-detection amplifiers are integrated into the modules to avoid data transmission problems between the radiometer and the electronics box. The sky and reference signals are at different levels, which are equalized after detection and integration by modulating the gain synchronously with the phase switch.

The thermal design is based on three principles: a) minimize the power dissipated in the focal assembly; b) maximize the effectiveness of radiative cooling by providing good views of cold space, and by intercepting conductive heat loads and radiating them away; c) segregate the warm and cold components, and keep them as far from each other as possible.

#### 4. MISSION PERFORMANCE AND SIMULATIONS

A large set of detailed simulation codes is being developed by both LFI and HFI Consortia, in close contact with the theoretical and hardware progress, with the aim of testing and contributing to improve the mission design. We briefly summarize here the basic concepts on several issues investigated through simulations.

A crucial effect is introduced by straylight, i.e., contamination from off-axis sources through the sidelobes of the instrument beam. Several sources of contamination, both instrumental and astrophysical, may introduce spurious signals. The primary environmental sources of error for the LFI are those due to imperfect off-axis rejection by the optical system of radiation from the Sun, Earth, Moon planets, and Galaxy. Sidelobe structure sweeping across the Galaxy can produce artifacts in any direction. Sidelobe contributions are dominated by the features relatively near the optical axis and typical maximum ratios between the sidelobe and the central beam signals reach levels of  $\simeq 10\%$  (Mandolesi et al. 1998, section 2.1.2); we require the level of galactic contamination be below the noise level with a factor of two margin to allow for uncertainties in the level of galactic emission. The exact contamination levels depend on the details of the sidelobe pattern, typically in the range  $-60$  to  $-70$  dB (for a more detailed study see Polegre et al. 1998). In addition, emission from near field objects may affect the anisotropy measurements, such as emission from the warm parts of the spacecraft or fluctuations of mirror and shield temperature.

Transistor gain fluctuations in the receivers introduce amplifier noise temperature fluctuations that dominate in generating instrumental drifts with a  $1/f$  noise spectrum (Seiffert et al. 1997). The LFI radiometer design minimizes this effect, but residual stripes may be present. Destriping algorithms (Delabrouille 1998, Bu-

rigana et al. 1997), based on the idea that the same position in the sky must give the same observed temperature for different satellite spin axis positions, are quite efficient in further reducing these stripes, provided that the crossings between pointing positions in the sky obtained by different satellite spin axis positions are spreaded enough in the sky. In terms of increased noise with respect to the case of receiver pure white noise, these destriping techniques allow to reduce the noise added by stripes from some tens percent to few percent. Even in the case in which the angle,  $\alpha$ , between the telescope optical axis and the satellite spin axis is constantly kept at  $90^\circ$ , the worst from this point of view, for the major part of LFI beams located at  $2^\circ \div 4^\circ$  from the telescope optical axis – but not close to the sky scanning direction – we find a good destriping efficiency. For on-axis beams (or, equivalently, for beams located close to the sky scanning direction), reducing the angle  $\alpha$  significantly improves the efficiency of these destriping methods. By working with maps at resolutions close to the Planck FWHM's, we find that an angle of  $85^\circ$  is a good compromise for having efficient destriping and, considering the spread of the projected beam positions on the sky, practically full sky coverage.

Stripes in the observed maps can be also introduced by thermal instabilities. The closer the spin axis remains to the Sun-Planck direction, the smaller are any temperature variation induced by departure from perfect cylindrical symmetry. Thermal design aims at producing both low temperatures for sensitivity and thermal stability for reducing drifts. Destriping algorithms can be applied also for reducing residual stripes due to thermal instabilities, which typically show a noise spectrum close to  $1/f^2$  (Delabrouille 1998).

The amplitude and the reduction in the data analysis of stripes introduced by thermal and gain fluctuations is related to the Planck observational strategy. Sinusoidal oscillations of the spin axis may produce significant variations of the illumination by the Sun, so introducing unwanted thermal instabilities. On the other hand, different kinds of spin axis “oscillations” in which the angle between the spin axis and the Sun-Planck direction is kept constant (like for example a precession motion of the spin axis around an axis constantly kept on the ecliptic plane) minimise this effect and can be useful in reducing the stripes even for on-axis beams in the case  $\alpha = 90^\circ$ .

On the other hand, the scanning strategy controls another important issue: only when  $\alpha$  is constant the distribution in the sky of the sensitivity per pixel is smooth, the global integration time per pixel increasing continuously from the ecliptic equators to the ecliptic poles. In the other cases, we can have large areas in sky where the sensitivity significantly varies from a pixel to another even for small changes of the position in the sky. This is exactly what we want to avoid to not complicate the data analysis, particularly in presence of foreground contamination.

As discussed in the introduction, the most important LFI channels from the cosmological point of view are at 70 and 100 GHz; in particular the 100 GHz channel presents the best LFI resolution. In the new symmetric configuration of the Focal Plane Unit (FPU) the LFI feeds are located in a ring around the telescope optical axis at about  $2^\circ \div 4^\circ$  from it. Therefore, the issue of the main beam optical

distortions is crucial, particularly at 100 GHz, the LFI channel where we want to reach a FWHM angular resolution of  $\simeq 10'$ , necessary for the cosmological goal, and where the optical aberrations are maximum, because of their increasing with the frequency.

## 5. TELESCOPE DESIGN

The optimization of the Planck telescope is one of the goals of the Planck Teams. For the present optical study we have considered the 100 GHz channel.

The baseline design (report on Phase-A, TICRA yellow report, etc..) is a 1292.4 mm projected aperture gregorian off-axis telescope satisfying the Dragone-Mizuguchi condition (Dragone 1978; Mizuguchi et al. 1978; Rush et al. 1990). This condition set the tilting of the subreflector axis with respect the main reflector axis in order to cancel the cross-polarization. Unfortunately, only in the center of the focal surface (null scan angle) this kind of design shows symmetrical beams. Beam aberrations (expecially coma aberration) rise when the feedhorn is located outside the center of the focal surface, and increase with the frequency and the distance from the optical axis. Since one of the most crucial effect of beam distortions is an angular resolution degradation with respect to the central beam, we have studied two configurations with increased main reflector apertures in order to improve the resolution of the beams. The first one has a projected aperture of 1492.4 mm, while the projected aperture of the second configuration is 1750.0 mm. All these configurations have the same subreflector of the 1292.4 mm baseline design, as well as the same overall focal ratio. This means that the angular geometry is preserved for all the designs and no relevant changes of the FPU arrangement are needed.

Among other possible design configurations, an alternative to the Dragone-Mizuguchi Gregorian off-axis solution (in short “Standard”) is represented by the Aplanatic Gregorian design (in short “Aplanatic”), firstly proposed by Mark Dragan and the LFI Consortium in order to reduce the coma and the spherical aberration on a large portion of the focal surface (Villa et al. 1998b). This new solution is obtained by changing the conic constants of both mirrors (both ellipsoids of rotation) in order to satisfy the Aplanatic Condition. Two configurations have been studied, with 1292.4 mm and 1492.4 mm projected aperture respectively. Details of all the considered configurations, sketched in Figure 2, are reported in Table 1.

To analyze a general dual reflector system a dedicated software has been implemented at Istituto TeSRE/CNR (Villa et al. 1998b). The code calculates the amplitude and phase distribution on a regular grid of points on the tilted aperture plane (normal to azimuth and elevation directions on the sky).

The amplitude is calculated starting from the feed pattern and takes into account the space attenuation.

The phase is derived by calculating the path length of each ray, from the corresponding point on the aperture plane grid up to the focal point previously calculated (minimizing the wave front error of the spot diagram). Performing the Fourier Transform of the spatial phase-amplitude distribution on the aperture plane, the

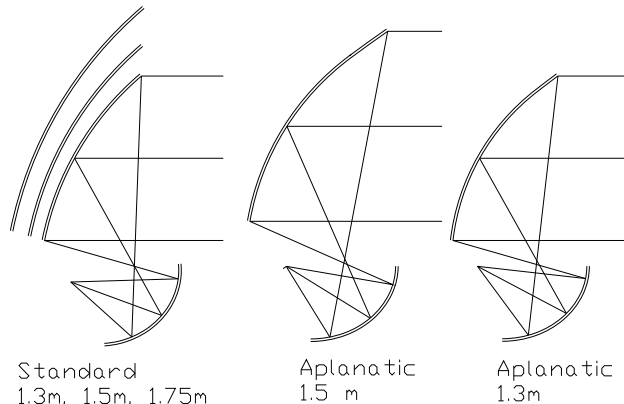


FIGURE 2. Schematic of the considered optical designs.

TABLE 1. Characteristics of the Telescopes: The first three configurations are Standard design. The last two are referred to the Aplanatic design.

Main Refl. Diameter (mm)	1292.4	1492.4	1750.0	1292.4	1492.4
Main Refl. Shape	Par.	Par.	Par.	Ell.	Ell.
Sub Refl. Tilting	14°	14°	14°	0°	0°
Sub Refl. Focal Length (mm)	514.29	514.29	514.29	680.912	688.858
Sub Refl. Shape	Ell.	Ell.	Ell.	Ell.	Ell.
Overall Focal Ratio	1.39	1.39	1.39	1.39	1.39

far field radiation pattern is readily obtained. For each configurations the contour plot of the normalized patterns as function of the sky-pointing scan angles (elevation, azimuth) have been calculated. Figure 3 shows our results for a typical beam position. Diffraction effects on the reflectors rim are not considered, but for the main beam response they are expected to be quite small.

All simulations have been done by considering the  $\cos^N(\theta)$  primary pattern with  $N = 91$  (for the Standard 1.3 m configuration this gives an edge taper of  $-30$  dB at  $22^\circ$  of angle).

In order to quantify the impact on the effective angular resolution,  $\text{FWHM}_{\text{eff}}$ , of the beams in CMB anisotropy measurements we have compared convolutions of a CDM anisotropy sky with the simulated beams and with a suitable grid of gaussian symmetric beams (see Burigana et al. 1998a and Mandolesi et al. 1997, section 3.2, for further details on the method). In Figure 4 we summarize our results for the five considered configurations. Note that the August 1998 ESA Baseline Planck telescope is a 1492.4 m aperture Gregorian telescope with the secondary (position, shape and size) still optimized for the 1.3 m Standard configuration: the main beam resolution is then equivalent to the 1.3 m Standard telescope.



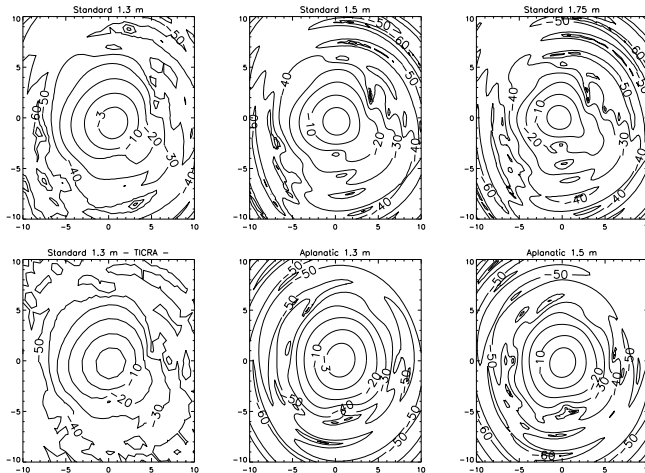


FIGURE 3. Contour plot of the normalized patterns of a beam located at  $El=+2^\circ$ ,  $Az=-2^\circ$  from the optical axis for the considered optical designs; also the pattern computed by TICRA for the 1.3 m standard telescope is shown for comparison. In each panel, the  $x$  and  $y$  axes are the standard U and V coordinates in radians (multiplied by 1000) in a reference roughly translated to the beam center.

The average of the  $FWHM_{\text{eff}}$  in the relevant regions (between  $\sim -2.5$  and  $\sim 2.5$  degrees for the 1.3m telescopes and between  $\sim -2$  and  $\sim 2$  degrees for the 1.5m telescopes) are similar for Standard and Aplanatic configurations with same aperture ( $\simeq 10$  arcmin for the  $\simeq 1.5$  m telescopes and even better for the 1.75 m telescope). On the other hand the  $FWHM_{\text{eff}}$  of beams located at angular distances from the center roughly equal or larger than  $\simeq 1^\circ$ , where typical Planck (LFI and also HFI) feeds are located, is somewhat better and also the spread of the  $FWHM_{\text{eff}}$ 's of the different beams is smaller for the Aplanatic configuration (Villa et al. 1998b).

We find that the beam shapes are more regular for the Aplanatic configuration, and, although elliptical, closer to gaussian shapes, due to the strong reduction of the coma. This could help also the reconstruction in flight of the beam pattern.

In addition, the Aplanatic configuration leads essentially unchanged the edge taper at the bottom edge of the main reflector ( $\sim -30\text{dB}$  for the central feed) compared to the Standard telescope, while it allows to improve the edge taper at the main reflector top edge ( $\sim -40\text{dB}$  for the central feed), where the spillover radiation is not shielded. This will most probably lead to an improvement of the top edge straylight.

This preliminary study suggests that the Aplanatic configuration can represent a significant improvement for the main beam properties compared to the Standard configuration, possibly decreasing the sidelobe contamination. Further studies which include straylight, focal surface and feed positioning optimization, and mirror

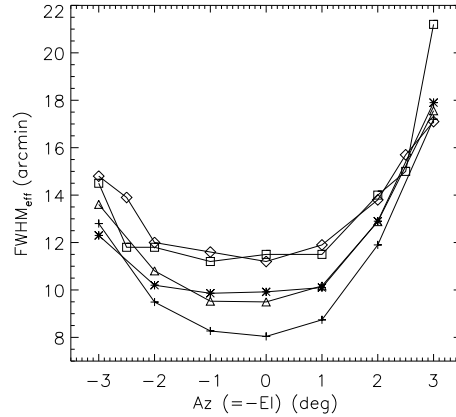


FIGURE 4. Effective FWHM of beams located at different distance from the optical axis along a diagonal on the sky field of view, for the considered configurations: the 1.3 m Standard telescope (diamonds), the 1.5 m Standard telescope (triangles), the 1.75 m Standard telescope (crosses), the 1.3 m Aplanatic telescope (squares) and the 1.5 m Aplanatic telescope (asterisks).

shapes, need to be done.

#### REFERENCES

- Bersanelli, M., et al. 1996, ESA, COBRAS/SAMBA Report on the Phase A Study, D/SCI(96)3  
 Bersanelli, M., et al. 1998, Experimental Astronomy, in press  
 Bersanelli, M., Mandolesi, N. 1998, this Conference  
 Bond, R.J., Efstathiou, G., Tegmark, M. 1997, MNRAS 291, L33  
 Burigana, C., et al. 1997, Int. Rep. TeSRE/CNR 198/1997  
 Burigana, C., et al. 1998a, A&ASS 130, 551  
 Burigana, C., et al. 1998b, this Conference  
 Cavaliere, A., Danese, L., De Zotti, G. 1979, A&A 75, 322  
 Delabrouille, J. 1998, A&ASS 127, 555  
 De Zotti, G., Toffolatti, L. 1998, this Conference  
 Dragone, C. 1978, B.S.T.J., Vol. 57, No. 7, 2663  
 Mandolesi, N., et al. 1997, Int. Rep. TeSRE/CNR 199/1997  
 Mandolesi, N., et al. 1998, Planck LFI, A Proposal Submitted to the ESA.  
 Mizuguchi, Y., Akagawa, M., Yokoi, H. 1978, Electronics & Comm. in Japan, Vol. 61-B, No. 3, 58  
 Myers, S.T, Baker, J.E., Readhead, A.C.S., Leitch, E.M., Herbig, T. 1997, ApJ 485, 1  
 Pasian, F., Gispert, R. 1998, this Conference  
 Polegre, A.M., et al. 1998, this Conference  
 Puget, J.-L., et al. 1998, HFI for the Planck Mission, A Proposal Submitted to the ESA.  
 Rephaeli, Y., 1995, ARA&A 33, 541  
 Rush, W.V.T., et al. 1990, IEEE Trans. AP., Vol. 38, No. 8, 1141  
 Seiffert, M., et al. 1997, The Review of Scientific Instruments, submitted  
 Toffolatti, L., et al. 1998, MNRAS 297, 117  
 Villa, F., Bersanelli, M., Mandolesi, N. 1997, Int. Rep. TeSRE/CNR 188/1997  
 Villa, F., Bersanelli, M., Mandolesi, N. 1998a, Int. Rep. TeSRE/CNR 206/1998  
 Villa, F., Mandolesi, N., Burigana, C. 1998b, Int. Rep. TeSRE/CNR 221/1998  
 Wade, L.A., Levy, A.R. 1997, Cryocoolers, 9, 587  
 Zaldarriaga, M., Spergel, D., Seljak, U. 1997, ApJ 488, 1